J. Am. Soc. Mass Spectrom. (2016) 27:59–72
DOI: 10.1007/s13361-015-1237-4

RESEARCH ARTICLE

Mechanistic and Kinetic Study of Singlet O_2 Oxidation of Methionine by On-Line Electrospray Ionization Mass Spectrometry

Fangwei Liu, Wenchao Lu, Xunlong Yin, Jianbo Liu

Department of Chemistry and Biochemistry, Queens College and the Graduate Center of the City University of New York, Queens, NY 11367, USA

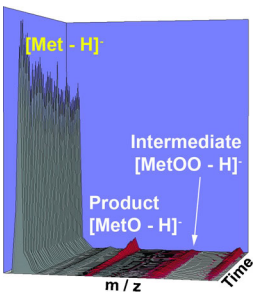

Abstract. We report a reaction apparatus developed to monitor singlet oxygen ($^1O_2$) reactions in solution using on-line ESI mass spectrometry and spectroscopy measurements. $^1O_2$ was generated in the gas phase by the reaction of H_2O_2 with Cl_2, detected by its emission at 1270 nm, and bubbled into aqueous solution continuously. $^1O_2$ concentrations in solution were linearly related to the emission intensities of airborne $^1O_2$, and their absolute scales were established based on a calibration using 9,10-anthracene dipropionate dianion as an $^1O_2$ trapping agent. Products from $^1O_2$ oxidation were monitored by UV-Vis absorption and positive/negative ESI mass spectra, and product structures were elucidated using collision-induced dissociation-tandem mass spectrometry. To suppress electrical discharge in negative ESI of aqueous solution, methanol was added to electrospray via in-spray solution mixing using theta-glass ESI emitters. Capitalizing on this apparatus, the reaction of $^1O_2$ with methionine was investigated. We have identified methionine oxidation intermediates and products at different pH, and measured reaction rate constants. $^1O_2$ oxidation of methionine is mediated by persulfoxide in both acidic and basic solutions. Persulfoxide continues to react with another methionine, yielding methionine sulfoxide as end-product albeit with a much lower reaction rate in basic solution. Density functional theory was used to explore reaction potential energy surfaces and establish kinetic models, with solvation effects simulated using the polarized continuum model. Combined with our previous study of gas-phase methionine ions with $^1O_2$, evolution of methionine oxidation pathways at different ionization states and in different media is described.

Keywords: On-line ESI mass spectrometry, In-spray solution mixing, Reaction kinetics, Methionine, Singlet oxygen, Persulfoxide, Sulfoxide, Photooxidation, DFT-PCM calculation

Received: 22 May 2015/Revised: /Accepted: 24 July 2015/Published Online: 26 August 2015

Introduction

Methionine (Met) is one of the five amino acids (the other four are tryptophan, tyrosine, histidine, and cysteine) that are most susceptible to the attack by reactive oxygen species (ROS) [1–3]. Oxidation of Met residues in proteins produces sulfoxides (MetO) [4–6]. Under extremely strong oxidative conditions, MetO can be irreversibly oxidized to sulfone (MetOSO) [3, 6]. It is well accepted that hydrophobic contacts via the Met residues contribute to protein stability. Moreover, Met has the propensity to interact with aromatic residues, and the resulting Met sulfur-aromatic motif provides additional stabilization over hydrophobic interactions [7]. Oxidation of Met to MetO decreases hydrophobicity [5] and disrupts both dispersion and electrostatic interactions present in the sulfur-aromatic motif [7]. Such oxidation-induced post-translational modifications may cause proteins to change conformations and lose functions [8–10], and are related to pathophysiological conditions such as cancer, aging, and neurodegenerative diseases [3, 11]. On the other hand, surface-exposed Met residues act as endogenous antioxidants or "molecular bodyguards" under oxidative stress, protecting other residues important to the functions of proteins [12, 13]. This is due to the fact that cells are capable of reducing MetO back to Met, catalyzed by Met sulfoxide reductases (Msrs) [14–16]. The reversible Met oxidation is also identified as a trigger for the functions of two protein

Electronic supplementary material The online version of this article (doi:10.1007/s13361-015-1237-4) contains supplementary material, which is available to authorized users.

Correspondence to: Jianbo Liu; *e-mail:* jianbo.liu@qc.cuny.edu

kinases CaMKII and transcription factor HypT (HOCl specific) [17, 18]. Consequently, the contents of Met and MetO in cells can be used to indicate the extent of ROS generation, and the activities of oxidant scavengers and Msrs.

Oxidation kinetics of Met to MetO has been investigated in the presence of various ROSs [3, 19–24], of which $^1O_2$-mediated kinetics was mostly measured using photooxidation methods [23, 24]. In these experiments, $^1O_2$ was generated via energy transfer from the triplet excited state of a sensitizer to $^3O_2$ (type II photosensitization) [25]. Photooxidation of Met [24, 26–32] depends on various parameters (e.g., pH, O_2 concentration, solvent composition, buffer ions, and combination of light and sensitizers). Determination of $^1O_2$-mediated oxidation kinetics was also challenged by the competition between radical- and $^1O_2$-mediated reactions, and the interaction between substrates and excited sensitizers.

To avoid the interferences in photooxidation experiments, one approach is to use heterogeneous photosensitization in which sensitizers are isolated from reaction solution and the sensitizer-generated $^1O_2$ is delivered through space [33] or via bubbles [34]. We have adopted another approach based on a chemical reaction to produce radical-free, "clean" $^1O_2$. Coupled with ion-beam-scattering methods and electrospray ionization mass spectrometry (ESI MS), we have investigated $^1O_2$-mediated oxidation dynamics of Met in the gas phase at different ionization and hydration states (including $[Met + H]^+(H_2O)_{0\text{-}2}$ and $[Met - H]^-(H_2O)_{0\text{-}2}$) [35, 36]. Study of the $^1O_2$ reactions with dehydrated $[Met + H]^+$/$[Met - H]^-$ has allowed us to identify the intrinsic interactions between Met and $^1O_2$; and that of the $^1O_2$ reactions with hydrated $[Met + H]^+(H_2O)_{1\text{-}2}$/$[Met - H]^-(H_2O)_{1\text{-}2}$ has enabled us to recognize the effects of individual solvent molecules. On the one hand, gas-phase findings provide fundamentals in understanding the oxidation mechanism; on the other hand, they suffice as valuable references in examining specific and continuum solvent effects, and it will be interesting to see how the gas-phase findings can be extrapolated to solution models. This prompted us to look at $^1O_2$ oxidation of Met in aqueous solution, aimed at investigating the resemblance and evolution of reaction pathways and products from the gas phase to aqueous continuum.

Over recent years, applications of ESI MS have spread rapidly in monitoring solution-phase reaction kinetics and probing the course of chemical transformations [37–39]. The fast growth of such applications relies on several exclusive advantages of ESI MS: (1) The ESI process is simple, "clean" and "soft", where no harsh conditions are applied to the sample solution being transferred into mass spectrometer. As a result, weakly bound species may be detected in the gas phase; (2) on-line ESI MS is a rapid and sensitive approach that detects multiple products simultaneously at very low concentrations (nanomolar), and provides chances for capturing short-lived intermediates, which might not survive the normal handling for off-line analysis; (3) each mass spectrum represents a snapshot of an on-going reaction, and kinetics can be measured through continuous analyses of the reaction mixture.

However, monitoring $^1O_2$ reaction kinetics in solution puts severe demands on an on-line ESI MS experiment, which warrants careful consideration in the design of the corresponding apparatus and methodologies. First, the reaction apparatus is continuously pumped in order to replace quenched O_2 in solution with fresh $^1O_2$; consequently, ESI MS has to sample solution from a low-pressure reaction system. Secondly, we need to record ESI MS of aqueous sample in both positive and negative modes. Note that water has a high surface tension that requires high ESI spray potentials. The high spray potentials may lead to the presence of conventional corona discharges at the ESI emitter. For otherwise equivalent conditions, a breakdown due to a corona discharge occurs at significantly lower field strength in the case of the negative polarity than in the case of the positive one, and the ESI operation becomes impossible without discharge suppression [40, 41]. However, the method to be used for discharge suppression should pose inappreciable interference with the aqueous sample. Thirdly, the sample transfer time must be minimized so that the reaction progress can be tracked promptly. To meet these specifications, a new on-line ESI MS and spectroscopy monitoring system was developed in the present work. Capitalizing on this apparatus, we have measured the reaction kinetics between Met and $^1O_2$ in different pH solutions. The results were interpreted with the aid of electronic structure calculations. Combined with the recently reported gas-phase dynamics of bare/hydrated Met ions with $^1O_2$ [35, 36], a sound understanding has been obtained for Met oxidation.

Experimental and Computational Details

$^1O_2$ Generation, Detection, and Reaction

$^1O_2$ was generated by the reaction of $H_2O_2 + Cl_2 + 2KOH \rightarrow O_2$ (~85% $X^3\Sigma_g^-$ and ~15% $a^1\Delta_g$) + 2KCl + $2H_2O$ [35, 42, 43]. As shown in Figure 1, 13 mL of 8 M KOH (85%, Alfa Aesar, Ward Hill, MA, USA) was added to 20 mL of 35 wt% aqueous H_2O_2 (Alfa Aesar) in a sparger (**1**), which was immersed in a chiller held at –19°C. The resulting mixture was degassed quickly. Then, 2.6 sccm of Cl_2 (≥99.5%, Sigma-Aldrich, St. Louis, MO, USA) was mixed with 96 sccm of He (Research grade, T.W. Smith, Brooklyn, NY, USA) and bubbled through the H_2O_2/KOH slush. All of the Cl_2 reacted with H_2O_2. The gaseous products passed through a cold trap (**2**, kept at –70°C) to remove water vapor. Only $^1O_2$, $^3O_2$ and He remained in the downstream gas. The concentration of $^1O_2$ in the gas was determined by measuring $^1O_2$ emission ($a^1\Delta_g \rightarrow X^3\Sigma_g^-$, $v = 0 - 0$) [44] at 1270 nm in an optical emission cell (**3**). Emission from the cell was collected using a plano-convex lens, passed through an optical chopper (SRS model SR540, Sunnyvale, CA, USA) and 5-nm bandwidth interference filter centered at 1270 nm, and focused by another plano-convex lens into a thermoelectrically cooled InGaAs detector (**4**, Newport model 71887, Irvine, CA, USA) coupled with a lock-in amplifier (SRS model SR830, Sunnyvale, CA, USA). $^1O_2$ (mixed with $^3O_2$ and He) was then bubbled into the aqueous solution in a reaction vessel (**5**). During the experiment, the entire apparatus was continuously pumped with a mechanical pump, and the

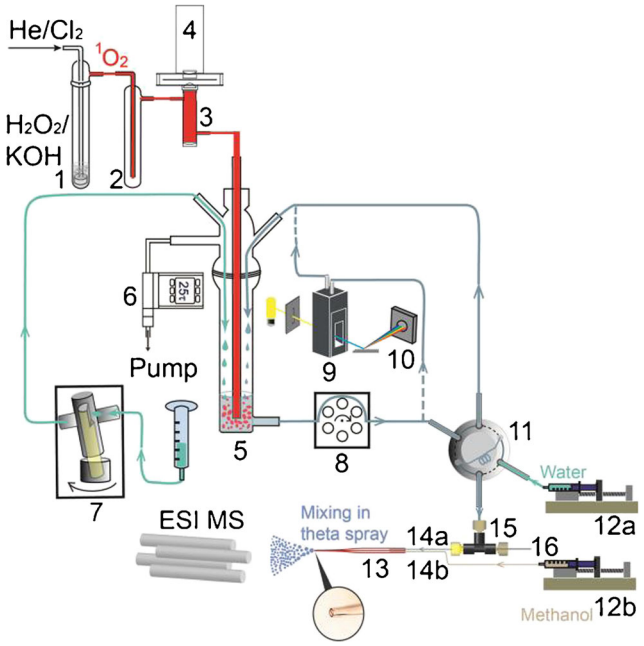

Figure 1. Schematic depiction of on-line coupling of $^1O_2$ generation, detection, and reaction to spectroscopy and ESI MS. The configuration of ESI is shown for negative ion mode. For positive ESI, aqueous solution from sampling loop is directly transferred to an ESI needle through PEEK tubing. **1**) Sparger; **2**) cold trap; **3**) optical emission cell; **4**) InGaAs detector; **5**) reaction vessel; **6**) pressure relay; **7**) piston pump; **8**) peristaltic pump; **9**) quartz flow cell; **10**) diode array spectrometer; **11**) 2-position switching valve; **12a/b**) syringe pump; **13**) borosilicate theta-glass capillary; **14a/b**) PEEK tubing; **15**) PEEK microtee; and **16**) platinum wire

pressure of the apparatus was maintained at 25 τ (slightly above water vapor pressure at room temperature) through a pressure relay (**6**, Cole-Parmer 00244OW, Vernon Hills, IL, USA). The pumping serves several purposes: reducing the residence time of $^1O_2$ in the gas phase and therefore minimizing its wall quenching and self-quenching, and removing quenched O_2 and replenishing fresh $^1O_2$ to the reaction solution. Since a significant amount of water evaporated from **5** at the low operating pressure, extra water was replenished into **5** through an Ismatec Reglo-CPF rotary piston pump (Glattbrugg, Switzerland) (**7**) at a precisely controlled flow rate.

To check the reactivity of aqueous substrates towards $^3O_2$/He, control experiments were performed under the same conditions as those for $^1O_2$, except that Cl_2 was replaced by O_2 (T.W. Smith, Brooklyn, NY, USA) gas at the same flow rate.

On-Line Sampling for Spectroscopy and ESI MS

Our monitoring system includes a UV-Vis spectrometer and an ESI tandem mass spectrometer. Absorption and mass spectra were recorded over the course of reactions. As illustrated in Figure 1, the aqueous reaction solution was circulated by a peristaltic pump (**8**) through a quartz flow cell (**9**, Starna Cells 583.65-Q-10/Z15, 1-cm path length, Atascadero, CA, USA). UV-Vis absorption was monitored using an Ocean Optics USB4000 diode array spectrometer (**10**, Dunedin, FL, USA). Spectra were recorded at 30-s intervals using the Ocean Optics SpectraSuite software.

To the best of our knowledge, most on-line ESI MS approaches sampled reaction solution at a pressure near atmospheric or higher, where the solution was delivered to ESI by gravity or positive gas pressure [45–51]. However, our reaction system needs to be maintained at a pressure of 25 τ as rationalized above. Therefore, one feature of our sampling system is to transport sample from low-pressure solution to open-air ESI, using a sampling loop (0.035 mL vol.) coupled to a 2-position switching valve (**11**). The valve was controlled by a LabVIEW program. For each measurement, the valve was placed in load position for 2 s to fill the loop with reaction solution through **8**, and then switched to injection position for transferring the solution to electrospray. The time lag between sample load and MS measurement is determined by the dead volume (~0.1 mL) of the transfer line connecting the sampling loop to ESI and the sample transfer rate. Note that a typical flow rate for ESI is 1 μL/min, which would result in far too long delay for kinetic measurements if this rate is used for sample transfer. In a previous on-line ESI MS experiment [52], we adopted Cooks and coworkers' method [51] by adding a splitter to the sample transfer line, right before ESI. The sample was swept to ESI under N_2 gas pressure. This configuration allowed for a high sample transfer rate (11.4 mL/h), and in the meantime delivered only a small fraction of the flow to ESI. We were able to reduce the sample transfer time to less than 30 s [52]. But this method increased the total sample volume needed (by a factor of ~200) for each measurement. In the present work, we developed another approach to reduce the lag time. The sampling loop was swept by water plug using a syringe pump (**12a**) at programmed flow rates. For each sampling, the flow rate of **12a** was first set to 6 mL/h. During this duration, the sample was loaded, inserted into the transfer line, and transferred to the ESI emitter. After that, the rate of **12a** decreased to 0.04 mL/h until the completion of MS measurement. In the positive ion mode, the ESI emitter was assembled by gluing the stainless steel hypodermic tubing (35-gauge, 0.005" o.d. × 0.002" i.d. × 0.5″ length, Small Parts Inc., Logansport, IN, USA) to the exit (PEEK tubing, 0.0625" o.d. × 0.007" i.d., IDEX, Oak Harbor, WA, USA) of **11**, and the total time for sample load and transfer was minimized to less than 10 s.

An issue for negative ESI of aqueous solution is electrical discharge. Due to the high surface tension of water, its ESI onset field strengths are $\pm 8.9 \times 10^6$ V/m in positive and negative ion modes, respectively (much higher than those of $\pm 5 \times 10^6$ V/m for methanol) [41]. Unfortunately, for the negative ion mode corona discharge at the stainless steel tip occurred at lower field strength than the ESI onset [41]. As a result, the stainless steel emitter could not be used in negative ESI. Cassou et al. reported negative nano-ESI of water solution by using borosilicate capillary with an ESI spray potential of –0.7 kV and a 3-mm distance between the emitter and the counter electrode [53]. We were not able to achieve stable ESI with the same field strength, presumably because of the higher flow rate we used. Our approach is to utilize a borosilicate theta-glass capillary (**13**,

Sutter Instrument, Novato, CA, USA) as an ESI emitter [54–56], and mix aqueous sample solution and methanol (HPLC grade, Fisher Scientific, Pittsburgh, PA, USA) at the tip of the emitter so as to lower ESI operating potential. Aqueous solution and methanol were individually delivered by syringe pumps **12a** and **12b** at a flow rate 0.01 and 0.03 mL/h, respectively, and directed into the two separated channels within the theta capillary through short PEEK tubing (**14a** and **14b**, 255 μm i.d. × 510 μm o.d.). The theta capillary was laser-pulled to a tip size of 20 μm i.d. × 40 μm o.d. by a micropipette puller (Sutter Instrument P-2000). A PEEK microtee (**15**, 0.1 μL dead volume, IDEX) was inserted to the aqueous sample line, and a platinum wire (**16**, 0.005" o.d., Alfa Aesar) was inserted into one stem of **15** to supply the electrical connection (–2.8 kV) for ESI. In this in-spray solution mixing, the encounter of aqueous solution and methanol took place at the time when solution reaction was terminated by spray. Consequently, interference with aqueous reactions by methanol was minimized, and diffusion and turbulence were avoided during fluid mixing.

ESI MS and Collision-Induced Dissociation-Tandem MS Measurements

A home-built guided-ion-beam tandem mass spectrometer was used for ESI MS measurements. The operation, calibration, and data analysis procedures for the mass spectrometer were described previously [57]. In brief, the apparatus consists of an ion source, radio frequency (rf) hexapole ion guide, quadrupole mass filter, rf octopole ion guide surrounded by a scattering cell, second quadrupole mass filter, and a pulse-counting detector. Both quadrupole mass filters use Extrel 9.5 mm tri-filter rods (Extrel CMS, Pittsburgh, PA, USA) and were operated at 2.1 MHz with a detectable *m/z* range of 1 to 500.

An ESI emitter was held at 3.7 and –2.8 kV, respectively, for producing positively and negatively charged species from sample solution. Charged droplets entered the source chamber of the mass spectrometer through a desolvation capillary (which was heated to 130°C and held at 100 V for positive ions and –120 V for negative ones). The distance between the emitter tip and the entrance of the desolvation capillary was 1 cm. Liquid droplets underwent desolvation as they passed through the heated capillary, converted to gas-phase ions in the source chamber. A skimmer with an orifice of 0.99 mm is located 3 mm from the capillary end, separating the source chamber and the hexapole ion guide. The skimmer was biased at 20 V for positive ions and –20 V for negative ones. Ions were transported into the hexapole at a pressure of 26 mτ, undergoing collisional focusing and cooling to 310 K. In conventional ESI MS measurements, the first quadrupole mass filter was rendered to an rf-only ion guide, and ions were mass-analyzed by the second quadrupole.

In order to identify the structures of product ions, collision-induced dissociation (CID) was performed. The product ions of interest were mass-selected by the first quadrupole, and then injected into the octopole ion guide, which trapped ions in the radial direction. DC bias voltage was applied to the octopole, allowing control of the kinetic energy (E_{lab}) of ions in the laboratory frame. E_{lab} can be converted to the collision energy (E_{col}) between ions and collision gas in the center-of-mass frame using $E_{col} = E_{lab} \times m_{neutral}/(M_{ion} + m_{neutral})$, where $m_{neutral}$ and M_{ion} are the masses of neutral collision gas and ions, respectively [58]. The octopole runs through the scattering cell filled with Xe gas (99.995%, Spectra Gases, Stewartsville, NJ, USA). The pressure of the cell was controlled using a leak valve and measured by a Baratron capacitance manometer (MKS model 690 head and 670 signal conditioner, MKS Instruments, Andover, MA, USA). CID was measured at E_{col} = 0.5, 1.0 and 1.5 eV with the cell pressure of 0.3 mTorr. Primary ions and fragment ions were collected by the octopole, and directed to the second quadrupole for mass analysis.

Electronic Structure Calculations

To aid in reaction mechanism interpretation, density functional theory (DFT) electronic structure calculations were performed using Gaussian 09 [59]. All structures were fully optimized at the B3LYP/6-31+G* level of theory. To take into account the solvation effects for aqueous reactants, transition states (TSs), intermediates, and products, we have employed the polarized continuum model (PCM) [60], which creates solute cavity via a set of overlapping spheres in the DFT calculations for all species. The DFT-PCM method has been successfully used for probing and reproducing the solution-phase chemistry of $^1O_2$ and peroxides, for example the $^1O_2$ oxidation of 6-thioguanine [61] and the transformation of 8-oxoguanine [62] in water. Conformation searching was conducted for all reactants, and their most stable confirmations were used as starting geometries in construction of reaction potential energy surfaces (PESs). All of the TSs were verified as first-order saddle points, and the vibrational mode with an imaginary frequency corresponds to the associated reaction pathway. All reported reaction energetics include zero-point energies (ZPEs) and thermal corrections at 298 K, with ZPEs scaled by a factor of 0.977 [63]. The energy barriers of TSs (with respect to reactants) were refined by single-point calculations at B3LYP/PCM/aug-cc-pVTZ using the B3LYP/PCM/6-31+G*-optimized reactants and TS geometries.

Results

$^1O_2$ Concentrations in Solution

In the experiment, chemically generated $^1O_2$ was continuously bubbled into aqueous solution in the reaction vessel. $^1O_2$ has a longer lifetime in the interior of bubbles (because of reduced encounters with water) than in bulk solution. After diffusing into the bulk water, $^1O_2$ has a lifetime of ~2 μs and can travel only ~150 nm [64]. Therefore, $^1O_2$ reactions occurred both at the gas/liquid interface of bubbles and in the bulk solution. Considering the steady concentration of airborne $^1O_2$ (as determined by the $^1O_2$ emission intensity, which varied within 10% over the course of reaction), and the continuous feeding of fresh $^1O_2$ into the reaction solution, a quasi-steady-state [$^1O_2$] may be assumed for

our reaction system as people did for bubbled $^1O_2$ in heterogeneous photosensitization [34]. In order to validate this assumption and determine the average value of $[^1O_2]$ in solution, two $^1O_2$ chemical trappers, 9,10-anthracene dipropionate dianion (ADPA, Chemodex Ltd., 9000 St. Gallen, Switzerland) and uric acid (99%, Alfa Aesar), were used as calibration compounds.

ADPA is known to react with $^1O_2$ chemically (i.e., without physical quenching), producing endoperoxide via [4+2] cycloaddition accompanied by bleaching of the absorption band of ADPA [65]. Figure 2a shows absorption changes of ADPA along the reaction course. The pH of the ADPA solution (0.05 mM) was maintained at 10.0 using borax/NaOH buffer. Shown in the insert of Figure 2a is the plot of $ln(A_t/A_0)$ versus reaction time, where A_t and A_0 are the ADPA peak absorption (at 378 nm) at different reaction times and time zero, respectively. The observation of a linear relationship between $ln(A_t/A_0)$ and reaction time indicates that consumption of ADPA obeys first-order rate law. Accordingly, an average $[^1O_2]$ in solution can be extracted using the reaction rate k_r (8.2×10^{-7} $M^{-1} \cdot s^{-1}$) for ADPA + $^1O_2$ [65].

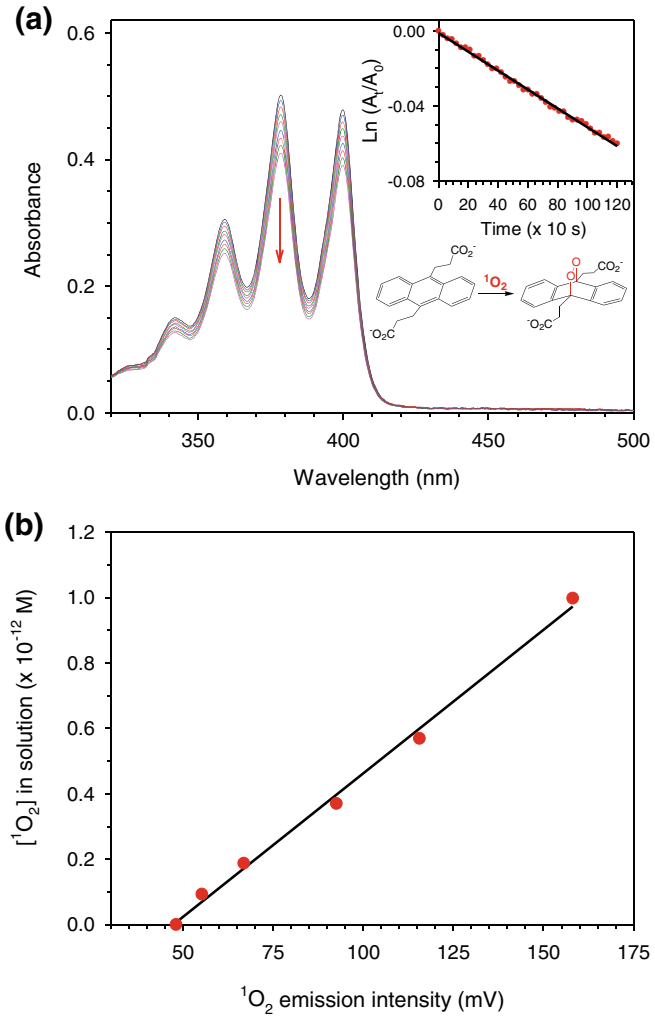

Figure 2. (**a**) UV-Vis absorption spectra of ADPA over the course of the reaction with $^1O_2$, recorded at pH 10. The insert shows the plot of $ln(A_t/A_0)$ versus reaction time, where A_t and A_0 are the absorbance at 378 nm at different times and time zero, respectively; and (**b**) the linear relationship between the emission intensity of airborne $^1O_2$ and the $[^1O_2]$ in solution determined using ADPA trapping

During each experiment, emission of airborne $^1O_2$ was continuously monitored. Figure 2b presents the correlation between the output of the emission detector and the corresponding ADPA-calibrated $[^1O_2]$ in solution. It shows that $[^1O_2]$ in solution increases linearly with the growth of airborne $^1O_2$ emission. The calibration curve crosses the x-axis at ~50 mV. This indicates a threshold airborne concentration below which all of the $^1O_2$ quenched in bubbling and diffusion before reaching aqueous substrates. In the subsequent experiments, the calibration curve of Figure 2b was used to determine $[^1O_2]$ in solution.

We also used uric acid [66–70] as a chemical trapper to test our reaction setup, and confirmed that $^1O_2$-induced uric acid oxidation follows first-order kinetics (see Supplementary Figure S1 in the Supporting Information). This further supports the pseudo-steady-state assumption for $[^1O_2]$ in our solution reactions. However, the literature reported k_r values for uric acid were based on bleaching of uric acid by photooxidation and did not represent exclusive chemical reactions with $^1O_2$. Montaña et al. [68] reported that both $^1O_2$-dependent and -independent mechanisms were involved in photobleaching of uric acid. Kanofsky [66] and Fischer et al. [67] found that uric acid was able to directly quench sensitizers. Rabello et al. [70] reported consecutive reaction steps for uric acid oxidation depending on sensitizers. For these reasons, the reported k_r of uric acid was not used for qualitative determination of $[^1O_2]$ in our experiment.

Met Oxidation Products, Mechanism, and Kinetics in Basic Solution

We present first the $^1O_2$ oxidation results of Met in basic solution. The reaction solution (pH = 10.4) was prepared by adding NaOH to 2.5 mM Met aqueous solution. Considering the pK values of Met (pK_a = 2.13 and pK_b = 9.28) [71], deprotonated $[Met - H]^-$ is the predominant species (i.e., 93% $[Met - H]^-$ versus 7% neutral Met) in this solution. Major product ions were found at m/z 164 and 313, corresponding to deprotonated sulfoxide $[MetO - H]^-$ and its Met adduct $[MetO - H]^-$-Met, respectively. As shown in Figure 3, the intensities of both products increase along the reaction time. Note that formation of dehydromethionine $[Met - 3H]^-$ was reported in the photooxidation of Met at pH 6 – 10 [24]. But no $[Met - 3H]^-$ was observed in our mass spectra.

It is possible that the product ions of m/z 164 have contribution from doubly charged covalently bound dimer $[Met - H]^-$-OO-$[Met - H]^-$. We have examined the isotope distribution at m/z 165, but did not observe obvious contribution from ^{34}S-containing $[Met - H]^-$-OO-$[Met - H]^-$. For further verification, we have carried out CID of the ions m/z 164 with Xe. If the ions were from $[Met - H]^-$-OO-$[Met - H]^-$, singly charged $[MetOO - H]^-$ would be expected in CID products. However,

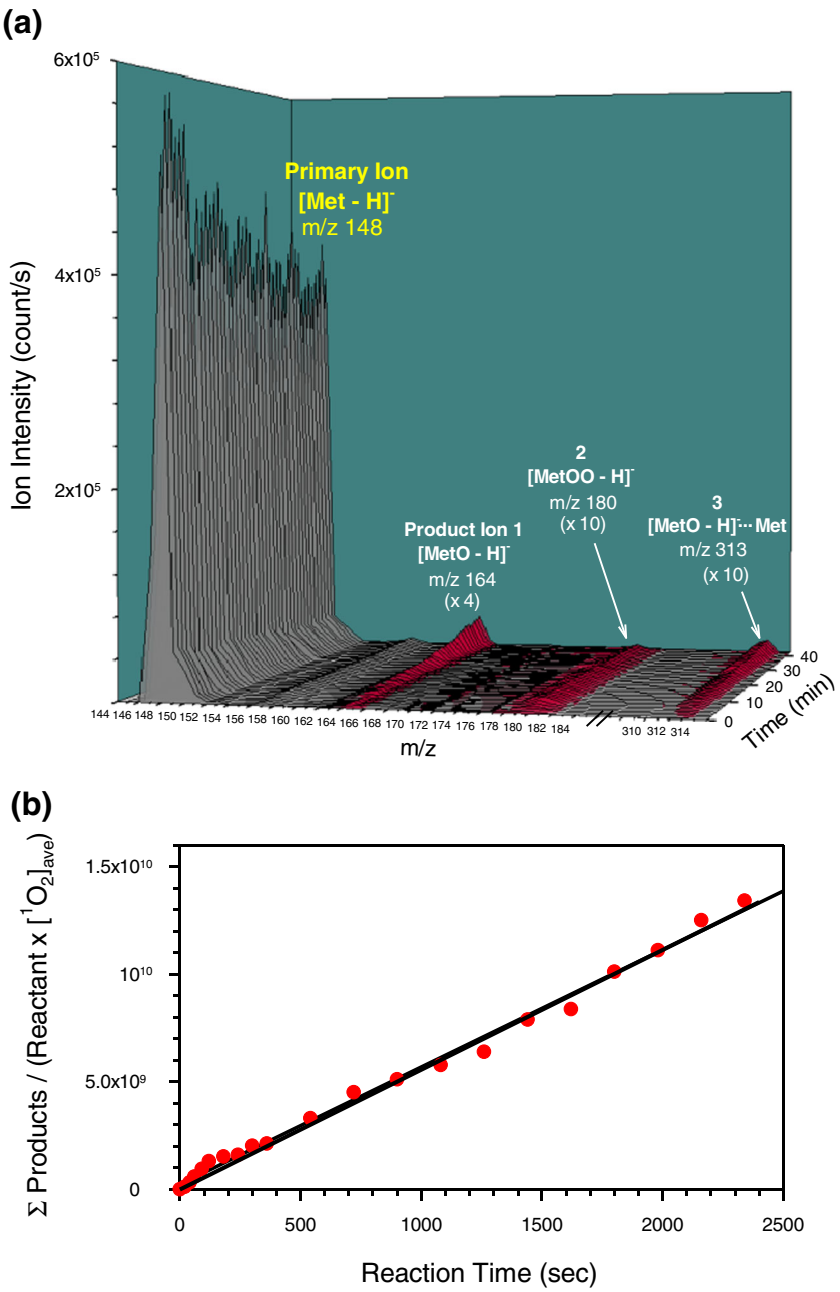

Figure 3. (**a**) Product mass spectra for Met oxidation in pH 10.4 solution at different reaction times; and (**b**) plot of $\frac{[[\mathrm{MetO}-\mathrm{H}]^-]}{[[\mathrm{Met}-\mathrm{H}]^-][^1\mathrm{O}_2]_{ave}}$ vs. reaction time t

no fragment ions were observed in the m/z range higher than 164 at E_{col} = 0.5 – 1.5 eV, ruling out this possibility.

CID of the product ions m/z 313 with Xe produced two fragment ions at m/z 164 and 148, which confirms that this species is an adduct of a neutral Met molecule to $[MetO - H]^-$. Our initial guess for the structure of $[MetO - H]^-$-Met was that the Met is covalently bonded to $[MetO - H]^-$ via S(=O)-S (thiosulfinate) or S-O-S linkage [72]. A grid search was then used to find global minima in their conformation landscapes. Each of the torsion angles of Met backbones was rotated systematically through 360° at 30° increments to generate trial staggered confirmations. To our surprise, all of the trial conformations converged to hydrogen-bonded structures of $[MetO - H]^-\cdots$Met. The most stable conformer lies 48.24 kJ/mol below the reactants, as shown in Scheme 1.

Our mass spectra also revealed a trace of ion signals at m/z 180 with no obvious time dependence after its initial rising. We have attributed this species to mainly persulfoxide $[MetOO - H]^-$. Persulfoxide is a common intermediate in the $^1O_2$ oxidation of dialkyl sulfide R_2S. However, persulfoxide readily reacts with a second R_2S to yield sulfoxide [73]. The species observed at m/z 180 could be the remaining $[MetOO - H]^-$,

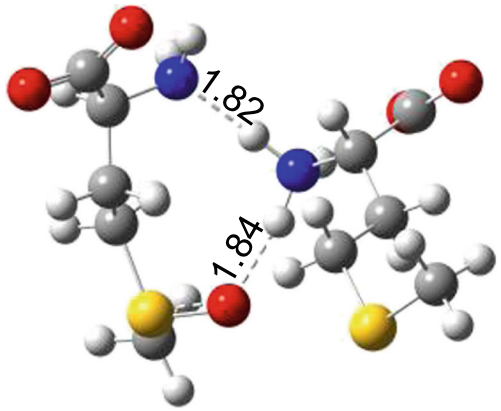

Scheme 1. Lowest-lying conformation of hydrogen-bonded [MetO – H]$^-$···Met

which survived on-line transfer. One complication in the interpretation of *m/z* 180 is that the [Met – H]$^-$/CH_3OH adduct was expected at the same *m/z* when methanol was added in negative ESI. To confirm the presence of [MetOO – H]$^-$, we repeated the experiment using ethanol as a supplementary solvent for ESI. The peak of *m/z* 180 was still visible in product mass spectra, verifying formation of [MetOO – H]$^-$. In Figure 3a, the contribution from [Met – H]$^-$/CH_3OH has been subtracted at *m/z* 180.

Note that an alternative structure for *m/z* 180 could be sulfone [MetOSO – H]$^-$. We have excluded this possibility for several reasons. It was reported that formation of sulfone occurs to a much lesser extent in Met oxidation [3, 6]. Based on DFT calculations, the reaction enthalpy for formation of [MetOSO – H]$^-$ is –367.6 kJ/mol with respect to [Met – H]$^-$ + $^1O_2$, which is more exothermic than that of [MetOO – H]$^-$. [MetOSO – H]$^-$, if it did form in the reaction, would have been observed in product mass spectra with considerable intensity. However, this is not the case in our measurements. The absence of sulfone could be due to a tight and high transition state (96.5 kJ/mol above the reactants, calculated at B3LYP/PCM/6-31+G*) for the interconversion from [MetOO – H]$^-$ to [MetOSO – H]$^-$.

To dissect the oxidation mechanism and elucidate the intermediacy of [MetOO – H]$^-$, we have mapped out the reaction PESs using relaxed PES scan at B3LYP/6-31+G*. Solvent effects were simulated using the PCM model. In PES calculations, the following reaction steps were assumed following Foote's sulfide photooxidation mechanism [74], of which the first step corresponds to formation of a key intermediate persulfoxide, and the with another [Met – H]$^-$ leading to two sulfoxides.

$$[\text{Met}-\text{H}]^- + {}^1\text{O}_2 \rightleftharpoons [\text{MetOO}-\text{H}]^- \qquad \Delta H_{rxn} = -62.7\ \text{kJ/mol} \qquad (1)$$

$$[\text{MetOO}-\text{H}]^- + [\text{Met}-\text{H}]^- \rightarrow 2[\text{MetO}-\text{H}]^- \qquad \Delta H_{rxn} = -245.1\ \text{kJ/mol} \qquad (2)$$

In Figure 4a, the potential energy for the first step is continuously monitored while the O_2 moiety is approaching the Met sulfur atom. The PES scan continuously varied the distance

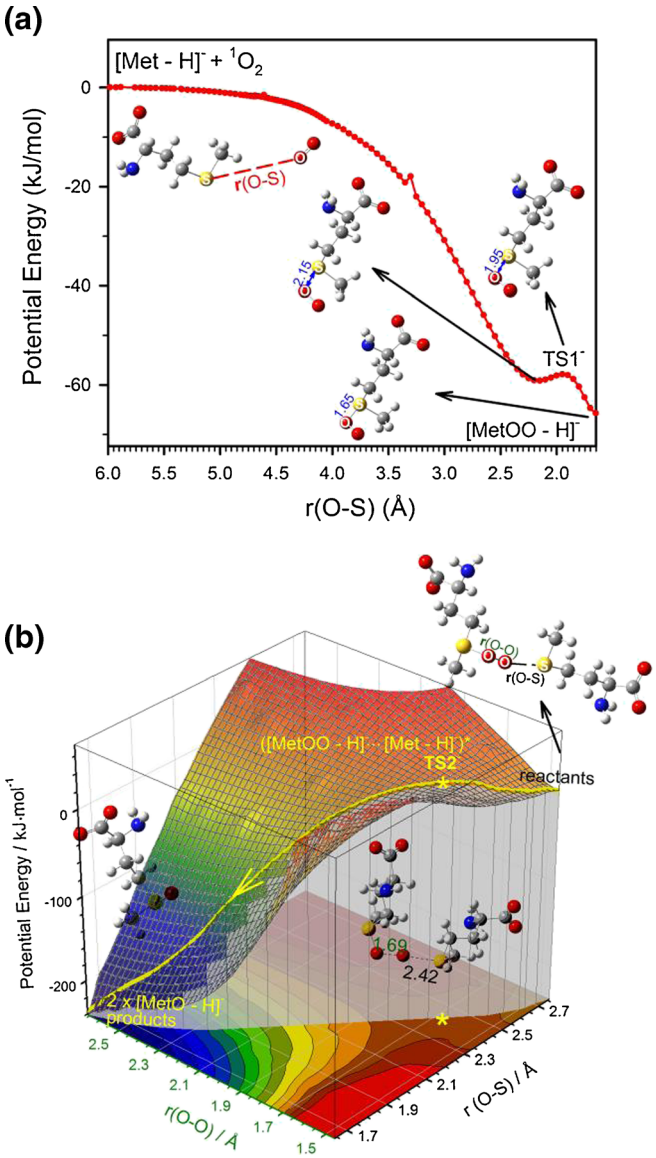

Figure 4. (**a**) PES for the reaction of [Met - H]$^-$ + $^1O_2$ → [MetOO – H]$^-$, plotted against the distance between the S atom of [Met – H]$^-$ and the closer O atom of O_2; and (**b**) 2D PES for the reaction of [MetOO – H]$^-$ + [Met – H]$^-$ → 2[MetO – H]$^-$, plotted against the O–O bond length and the distance between the terminal O of [MetOO – H]$^-$ and the S of [Met – H]$^-$. Calculations were carried out at B3LYP/PCM/6-31+G*

between S and the "closer" oxygen atom of O_2 at a step size of 0.05 Å from 6.0 Å to 1.65 Å until a stable [MetOO – H]$^-$ structure formed. All coordinates other than r(O-S) were optimized at each step. As illustrated in the PES, there are no activation barriers above reactants leading to formation of [MetOO – H]$^-$. The reaction initially forms a weakly bound precursor complex with r(O-S) of 2.15 Å. This electrostatic interaction-based precursor crosses over a small barrier TS1$^-$ at r(O-S) of 1.95 Å, evolving to a covalently bound product [MetOO – H]$^-$,which locates 62.7 kJ/mol below the isolated reactants.

Figure 4b shows a 2D PES for the second step reaction along the reaction coordinates r(O-S) and r(O-O). r(O-S) is the distance between the terminal O atom of $[MetOO - H]^-$ and the S atom of $[Met - H]^-$, and r(O-O) is the peroxide bond length of $[MetOO - H]^-$. These coordinates were chosen because r(O-S) describes the approach of reactants, while r(O-O) corresponds to the separation into two $[MetO - H]^-$ products. The PES was fit to nearly 700 points calculated at B3LYP/PCM/6-31+G*, and we optimized all other coordinates at each point. On this 2D surface, there is one activation barrier ($TS2^-$) located at the bottleneck leading from the reactants to the product well, with r(O-O) ~1.69 Å, r(O-S) ~2.42 Å, and an energy of 38.6 kJ/mol in excess of the reactants. This barrier accounts for the energy required to dissociate peroxy linkage and transfer the terminal O to the S of the approaching $[Met - H]^-$. The reaction enthalpy for Equation (2) is calculated to be –245.1 kJ/mol.

Analysis of the PESs provides insight into the Met oxidation mechanism in basic solution. Particularly, it verifies Equations (1) and (2) as two consecutive elementary steps. Both steps are bimolecular reactions, and the second one acts as the rate-limiting step due to the associated high-energy $TS2^-$. We therefore conclude that formation of $[MetOO - H]^-$ is much faster than its subsequent conversion to $[MetO - H]^-$. Note that $[MetOO - H]^-$ always presented low abundance in products. As illustrated in the product time profiles of Figure 3, the abundance of $[MetOO - H]^-$ rose from zero after the initial induction period and then had no obvious change during the major part of the reaction. Under these conditions, we made quasi-steady-state approximation (QSSA) [75] for $[MetOO - H]^-$, i.e.,

$$\frac{d[[MetOO-H]^-]}{dt} = k_1^-[[Met-H]^-][^1O_2] - k_{-1}^-[[MetOO-H]^-] - k_2^-[[MetOO-H]^-][[Met-H]^-] = 0, \quad (3)$$

where the rate constants k_1^- and k_{-1}^- are for the forward and backward reactions of Equation (1), and k_2^- for Equation (2). The reverse direction of Equation (1) represents a fraction of $^1O_2$ physical quenching that takes place via decomposition of $[MetOO - H]^-$, partially accounting for the reaction inefficiency [76]. $[Met - H]^-$ does not have an appropriate low-lying excited state to deactivate $^1O_2$ by electronic energy transfer, and a charge-transfer quenching mechanism is unlikely due to its large reaction endothermicity [36]. On the other hand, movement along the PES for $[Met - H]^- + {}^1O_2 \rightarrow [MetOO - H]^-$ may bring the persulfoxide into a region near the rapidly rising triplet state PES where intersystem crossing could occur [76]. A similar physical quenching mechanism was observed in the gas-phase collisions of $^1O_2$ with hydrated and dehydrated $[Met - H]^-$ [36].

Considering Equation (2) is rate-limiting, the steady state concentration of $[MetOO - H]^-$ implies that a large fraction of $[MetOO - H]^-$ must decay back to reactants rather than converted to $[MetO - H]^-$ (i.e., $k_{-1}^-[[MetOO - H]^-] \gg k_2^-[[MetOO - H]^-][[Met - H]^-]$). We can therefore eliminate $k_2^-[[MetOO - H]^-][[Met - H]^-]$ in Equation (3). This leads to a pre-equilibrium for Equation (1) as expressed by Equation (4), where K^- is the equilibrium constant.

$$[[MetOO-H]^-] = \frac{k_1^-[[Met-H]^-][^1O_2]}{k_{-1}^-} = K^-[[Met-H]^-][^1O_2] \quad (4)$$

The rate law for formation of $[MetO - H]^-$ can now be given as

$$\frac{1}{2}\frac{d[[MetO-H]^-]}{dt} = k_2^-[[MetOO-H]^-][[Met-H]^-] = K^-k_2^-[[Met-H]^-]^2[^1O_2] = k^-[[Met-H]^-]^2[^1O_2], \quad (5)$$

where k^- is the effective rate constant ($M^{-2}\ s^{-1}$). Among the three products ($[MetO - H]^-$, $[MetOO - H]^-$ and $[MetO - H]^- \cdots Met$), $[MetOO - H]^-$ is minimal (<0.1% over a period of 40 min) and can be safely ignored in the total product concentration. $[MetO - H]^- \cdots Met$ originates from the secondary reaction of $[MetO - H]^-$, and was lumped together with $[MetO - H]^-$ in calculating the total $[MetO - H]^-$ concentration. As a result, Equation (5) can be approximated as

$$\frac{d[[MetO-H]^-]}{dt} = 2k^-\left([[Met-H]^-]_0 - [[MetO-H]^-]\right)^2[^1O_2] \quad (6)$$

and its integrated form as

$$\frac{1}{[[Met-H]^-]_0 - [[MetO-H]^-]} - \frac{1}{[[Met-H]^-]_0} = 2k^-[^1O_2]dt \quad (7)$$

or

$$\frac{[[MetO-H]^-]}{[[Met-H]^-][^1O_2]_{ave}} = 2k^-[[Met-H]^-]_0 t \quad (8)$$

At the reaction time t, $\frac{[[MetO-H]^-]}{[[Met-H]^-]}$ can be measured using the relative abundances of reactant and product intensities in the corresponding mass spectrum. $[^1O_2]_{ave}$ was averaged over the integration period from 0 to t. As shown in Figure 3b, the plot of $\frac{[[MetO-H]^-]}{[[Met-H]^-][^1O_2]_{ave}}$ versus t fits into a linear relationship, supporting the proposed mechanistic scheme. The measured value of k^- is $1.0 \times 10^9\ M^{-2}\cdot s^{-1}$.

In the above two-step scheme, formation of $[MetO - H]^-$ can also be viewed as a trimolecular reaction that avoids nearly simultaneous three-body collisions [77]. Assuming k_2^- follows the Arrhenius equation with the activation energy E_2^- equal to $TS2^-$ (38.6 kJ/mol), the overall activation energy E_a^- for this trimolecular reaction is given by Equation (9) [77]. Since the ΔH_{rxn1} for the first step is –62.7 kJ/mol and the activation

energy for the second step is not too high, E_a^- for this trimolecular reaction becomes negative:

$$E_a^- = RT^2 \frac{d\ln K^-}{dT} + RT^2 \frac{d\ln k_2^-}{dT} = \Delta H_{rxn1} + E_2^- = -24.12 \ kJ/mol \quad (9)$$

Met Oxidation Products, Mechanism, and Kinetics in Acidic Solution

The oxidation product of Met in pH 3.2 solution (prepared by adding equimolar HCl to 0.5 mM Met aqueous solution) was detected at *m/z* 166 only, and its intensity increased with the reaction time as shown in Figure 5a. This product can be attributed to protonated $[MetO + H]^+$ or $[Met + H]^+$-OO-$[Met + H]^+$. We have performed CID of *m/z* 166 with Xe, and expected that $[Met + H]^+$-OO-$[Met + H]^+$ would lose a proton in CID. However, no $[Met + H]^+$-OO-Met was observed in CID, indicating that no $[Met + H]^+$-OO-$[Met + H]^+$ was formed in the reaction.

Note that due to the low carboxyl pK_a of Met, the percentile populations of neutral and protonated Met in pH 3.2 solution are 92% and 8%, respectively. As a result, the kinetics at pH 3.2 represents the oxidation chemistry of neutral Met (in a zwitterionic structure), albeit that the reactant and products were protonated in positive ESI spray. Therefore, the following kinetics discussion focuses on neutral Met. Similar as its deprotonated counterpart, we may propose two steps for oxidation of neutral Met. Their reaction enthalpies were calculated at the B3LYP/PCM/6-31+G* level of theory:

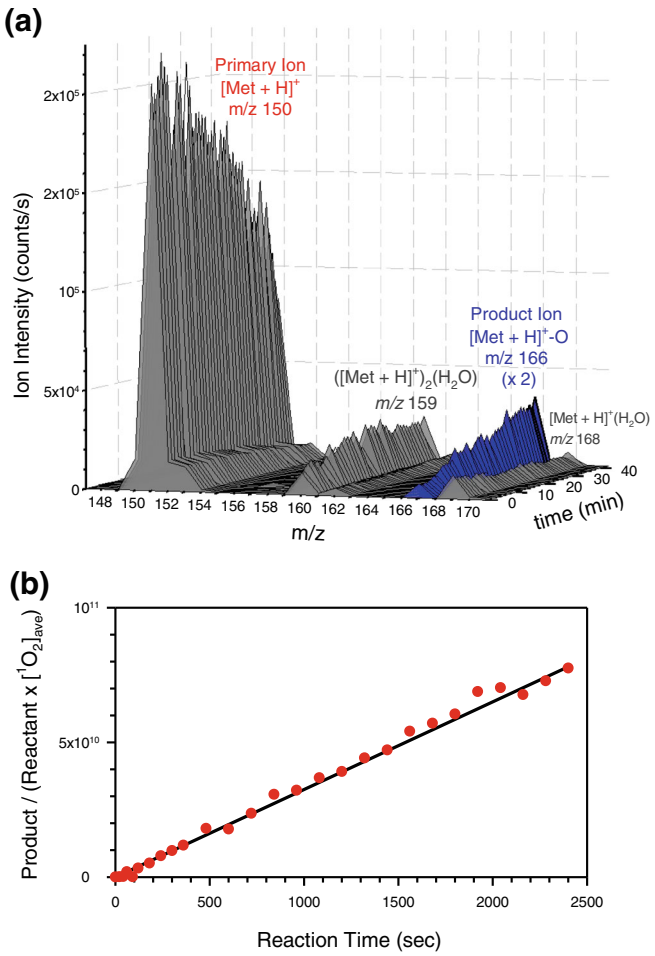

Figure 5. (**a**) Product mass spectra for Met oxidation in pH 3.2 solution at different reaction times; and (**b**) plot of $\frac{[MetO]}{[Met][^1O_2]_{ave}}$ vs. reaction time *t*

$$Met + {}^1O_2 \rightleftharpoons MetOO \qquad \Delta H_{rxn} = -83.0 \ kJ/mol \quad (10)$$

$$MetOO + Met \rightarrow 2MetO \qquad \Delta H_{rxn} = -244.1 \ kJ/mol \quad (11)$$

Concerning the reaction enthalpies for formation of persulfoxide and sulfoxide, the neutral system has only moderate changes compared to $[Met - H]^-$. More pronounced effects are observed in their PESs and associated activation barriers. Unlike the reaction of $[Met - H]^- + {}^1O_2$ (see Figure 4a), the PES scan for $Met + {}^1O_2$ (see Figure 6a) results in a covalently bound persulfoxide MetOO barrierlessly, without formation of a weakly bound precursor. MetOO has the O_2 moiety sandwiched between the ammonium group and the sulfur atom. MetOO has a zwitterionic character [76], so the proton of the ammonium group is shared between the N and the terminal O, rendering MetOO an "S-hydroperoxide" compound.

When another Met approaches MetOO, the latter transfers an O atom to Met. As the O–O bond ruptures and the new O–S bond forms, two molecules of MetO are produced. The PES for this process is scanned in Figure 6b along the distance between the terminal O of MetOO and the S of Met from 5.0 Å to 1.5 Å at a decrement of 0.05 Å each step. A transition state TS2 is located at r(O-S) of 2.37 Å and r(O-O) of 1.69 Å. At TS2, the O–O bond rupture is accompanied by the proton shuttling back to the amino group. TS2 lies 25.1 kJ/mol above the reactants (For comparison, TS2 is 13.5 kJ/mol lower than the corresponding $TS2^-$ for $[MetOO - H]^- + [Met - H]^-$). The overall activation energy E_a for $2Met + {}^1O_2 \rightarrow 2MetO$ is –57.9 kJ/mol according to Equation (9).

Based on the similarities between the PESs for $^1O_2$ with deprotonated and neutral Met, we conclude that both systems follow similar kinetics, and have applied the pre-equilibrium assumption to Equation (10) and QSSA to MetOO. As a result, the rate law for formation of MetO can be written as

$$\frac{1}{2}\frac{d[MetO]}{dt} = k_2[MetOO][Met] = \frac{k_1}{k_{-1}}k_2[Met]^2[{}^1O_2] = Kk_2[Met]^2[{}^1O_2] = k[Met]^2[{}^1O_2] \quad (12)$$

and its integrated form

$$\frac{[MetO]}{[Met][{}^1O_2]_{ave}} = 2k[Met]_0 t \quad (13)$$

where k_1 and k_{-1} are the rate constants for the forward and

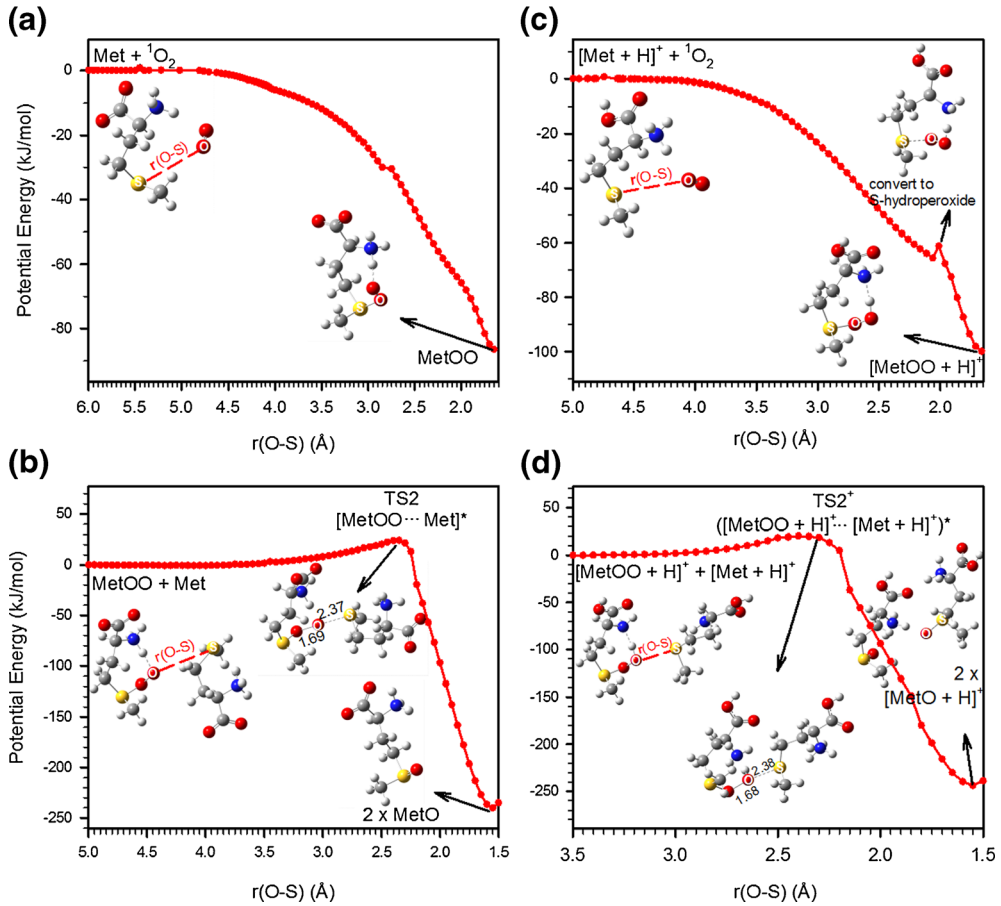

Figure 6. (**a**) PES for the reaction of Met + $^1O_2$ → MetOO, plotted against the distance between the Met S atom and the closer O atom of O_2; (**b**) PES for the reaction of MetOO + Met → 2MetO, plotted against the distance between the terminal O of MetOO and the S of Met; (**c**) and (**d**) are similar to (**a**) and (**b**), except that the Met, persulfoxide, and sulfoxide are protonated in (**c**) and (**d**). Calculations were carried out at B3LYP/PCM/6-31+G*

backward reactions of Equation (10), k_2 is the rate constant for Equation (11), K is the equilibrium constant for Equation (10), k is the effective rate constant for formation of MetO from 2Met + $^1O_2$, and $[Met]_0$ is the initial Met concentration. Note that to facilitate comparisons, all the corresponding rate constants, equilibrium constants, and barriers for different ionization states have been assigned identical names, but with "+/–" superscripts to indicate ionization states. Because of the lower TS2 barrier and consequently the larger k_2 (compared with $TS2^-$ and k_2^-, respectively), MetOO could react more promptly with another Met to yield MetO, and itself was therefore missing in product mass spectra. A plot of $\frac{[MetO]}{[Met][^1O_2]_{ave}}$ versus reaction time shown in Figure 5b is linear, from which the value of k is calculated to be $3.7 \times 10^{10}\ M^{-2}\cdot s^{-1}$. Remarkably, the k for neural Met is a factor of 37 higher than the k^- for deprotonated Met.

[Met + H]$^+$ Presents Similar Oxidation Behaviors as Neutral Met

To further explore the effects of ionization on the Met reaction with $^1O_2$, we have constructed the PESs for protonated [Met + H]$^+$ + $^1O_2$ in solution, as illustrated in Figure 6c and d. The oxidation of [Met + H]$^+$ follows the same reaction mechanism and shows nearly identical PES profiles and energetics as those for neutral Met, i.e., formation of S-hydroperoxide from encounter of [Met + H]$^+$ and $^1O_2$, followed by transfer of an O atom from [MetOO + H]$^+$ to another [Met + H]$^+$ via an activation barrier $TS2^+$ located at 27.0 kJ/mol above reactants.

$$[Met + H]^+ + {}^1O_2 \rightleftharpoons [MetOO + H]^+ \qquad \Delta H_{rxn} = -96.5\ kJ/mol \tag{14}$$

$$[MetOO + H]^+ + [Met + H]^+ \rightarrow 2[MetO + H]^+ \qquad \Delta H_{rxn} = -235.4\ kJ/mo \tag{15}$$

Discussion

Comparison with Photooxidation Kinetics

Matheson et al. [22] reported the reactive rate constant k_r ($1.6 \times 10^7\ M^{-1}\ s^{-1}$) and the total quenching rate constant k_t (1.7×10^7

M^{-1} s^{-1}) of $^1O_2$ with Met, where $^1O_2$ was generated by direct excitation of $^3O_2$ in D_2O (pD = 8.4). k_t was evaluated by competitive inhibition of the chemical reaction of bilirubin with $^1O_2$, and k_r was measured from loss of Met using an amino acid analyzer. Most of the other kinetic measurements for Met with $^1O_2$ are based on dye-sensitized photooxidations. Kraljic and Sharpatyi [78] reported a k_r of 8.6×10^6 M^{-1} s^{-1} in neutral water, according to O_2 consumption in steady state photosensitization. Lindig and Rodgers [79] examined k_t in neat D_2O using laser flash photolysis. Quenching of $^1O_2$ lay in the competition for $^1O_2$ between ADPA and Met, and the k_t for Met was measured to be 1.5×10^7 M^{-1} s^{-1}. In the experiment of Miskoski and García [23], $^1O_2$ was generated by rose bengel and tryptophan was used as a sacrificial substrate. The solution was photolyzed, and tryptophan consumption was monitored by its fluorescence in the absence and the presence of Met. Through a Stern-Volmer analysis of dynamic quenching of fluorescence, a k_t of 2.1×10^7 M^{-1} s^{-1} was obtained for Met at pH 7. k_r was measured based on O_2 consumption in a solution containing sensitizer and Met, and its value equals k_t. Based on a similar fluorescence quenching approach with diphenylfuran as a fluorescence probe, Sysak et al. reported a k_r of 1.15×10^7 M^{-1} s^{-1} in water (pH = 7) [24].

In the above works, no kinetic model was given and all of the k_r values were reported as a second-order rate constant in the unit of M^{-1} s^{-1}. If we assumed that formation of MetOO is the rate-limiting step for Met oxidation, the rate law for formation of MetO would follow second-order kinetics as Equation (16). Least-square fitting of our kinetics data to Equation (16) gave a k_1 value of 1.6×10^7 M^{-1} s^{-1}, similar as those reported from photooxidations. But our data were poorly fitted to Equation (16), suggesting Equation (16) does not describe kinetics correctly.

$$ln\frac{[Met]_0}{[Met]_0-[MetO]} = 2k_1\left[^1O_2\right]_{ave}t \quad (16)$$

The pH dependence of Met photooxidation has also been subjected to scrutiny. Earlier work on methylene blue-sensitized photooxidation of Met by Weil [80] and Spikes and MacKnight [27] showed a remarkable increase of O_2 consumption at a high pH range starting from 8. Sysak et al. [24] reported comprehensive pH dependence of Met photooxidation. According to them, the reaction is initialized by formation of a persulfoxide intermediate, followed by secondary reactions that are both pH- and buffer-dependent. At high pH (above 9) and catalyzed by buffer ions, OH^- may attack the S of persulfoxide, and the reaction gives one molecule of sulfoxide and one molecule of H_2O_2. At intermediate pH of 6–10, when Met carries a free amino group, the dominant pathway leads to dehydromethionine and H_2O_2 via internal displacement, where the dehydromethionine was assigned as a five-membered heterocyclic N-S compound [24]. Dehydromethionine may slowly hydrolyze to Met sulfoxide. At pH below 6, the persulfoxide oxidizes a second Met by the sulfide trapping mechanism, resulting in a stoichiometry of $2Met + {}^1O_2 \rightarrow 2MetO$. Competition among the secondary reactions accounts for the variation in O_2 uptake at different pH (i.e., the Met to $^1O_2$ ratio is 0.85:1 above pH 8 and 2:1 below pH 5 [24, 65]).

It is worth mentioning that formation of dehydromethionine in photooxidations was usually determined based on $–NH_2$ loss (using fluorogenic detection), but the loss of primary $–NH_2$ reactivity strongly depended on dyes [81] and buffer ions [24]. For example, little change was observed in the $–NH_2$ reactivity when eosin rather than methylene blue was used as a sensitizer [81]. It was suspected that the excited dye abstracted H atom from Met to form dehydromethionine [24, 80]. This hypothesis was corroborated by the fact that H_2O_2 was formed in methylene blue radical-mediated photooxidation of Met [80]. This implies that formation of dehydromethionine and H_2O_2 might not be completely $^1O_2$-specific [24], and the observed photooxidation pH dependence may reflect the oxidation-reduction potential between Met and excited dyes [80]. The uncertainty in photooxidation kinetics also remains as to whether the O_2 uptake is dedicated to $^1O_2$-induced oxidation or partially due to formation and reactions of $\cdot O_2^-$ with substrates. Such uncertainty was eliminated in our measurements, by bubbling "clean" $^1O_2$ to the Met solution, and using a straightforward MS technique to identify products.

Evolution of Met Oxidation from the Gas Phase to Solution

Preceding the present solution work, we reported the reactions of Met ions with $^1O_2$ in the gas phase. We first investigated the oxidation of protonated and deprotonated Met in the absence of water [35, 36]. The reaction systems were then augmented by adding explicit number of water ligands [35, 36], which accounts for microsolvation. The parallel gas- and solution-phase study helps us evaluate evolution of Met oxidation dynamics and kinetics from the gas phase, through microsolvation, to the aqueous solution.

The gas-phase oxidation processes follow an addition/elimination mechanism. The first step is addition of the O_2 moiety to the Met sulfur, yielding persulfoxide. The reaction outcome is determined by whether the persulfoxide intermediate has accessible product channels or not. In the case of dehydrated $[Met + H]^+ + {}^1O_2$, the persulfoxide intermediate evolves to an S-hydroperoxide $HN_2CH(CO_2H)CH_2CH_2S(OOH^+)CH_3$. The latter eliminates H_2O_2, yielding a dehydro compound of $MetH^+$. The reaction is extremely efficient at low E_{col}, approaching the collision limit. In the reaction of dehydrated $[Met - H]^-$, the persulfoxide intermediate interconverts to S-hydroperoxides

$NH_2CH(CO_2^-)CH_2CH_2S(OOH)=CH_2$ and $NH_2CH(CO_2^-)CH_2CH=S(OOH)CH_3$. Contrary to the protonated case, H_2O_2 elimination of deprotonated S-hydroperoxides encounters insurmountable barriers. Therefore, none of the deprotonated S-hydroperoxides could convert to stable end-products but decayed back to reactants, making $[Met - H]^-$ nonreactive towards $^1O_2$.

The fates of S-hydroperoxide intermediates are changed once $[Met + H]^+$ and $[Met - H]^-$ become hydrated. The dissociation of water ligand(s) provides an energy disposal path to release the heat gained from peroxide formation. It enables the capture of the "relaxed" S-hydroperoxides as stable end-products, i.e., $HN_2CH(CO_2H)CH_2CH_2S(OOH^+)CH_3$ for oxidation of $[Met + H]^+(H_2O)_{1,2}$, and

$NH_2CH(CO_2^-)CH_2CH_2S(OOH)=CH_2$ and $NH_2CH(CO_2^-)CH_2CH=S(OOH)CH_3$ for $[Met - H]^-(H_2O)_{1,2}$. For the reactions of $[Met + H]^+(H_2O)_{1,2}$, H_2O_2 elimination becomes less dominant.

Interestingly, reaction efficiencies of $[Met + H]^+(H_2O)$ and $[Met + H]^+(H_2O)_2$ are 15 and 25 times higher than those of $[Met - H]^-(H_2O)$ and $[Met - H]^-(H_2O)_2$, respectively. The effect of ionization state on gas-phase reaction efficiencies can be traced back to the formation efficiencies of protonated and deprotonated S-hydroperoxides, whose structures are completely different. Formation of protonated S-hydroperoxide $HN_2CH(CO_2H)CH_2CH_2S(OOH^+)CH_3$ takes places via intramolecular proton transfer from the $[Met + H]^+$ ammonium group to –SOO, and there is no activation barrier. On the other hand, deprotonated S-hydroperoxide $NH_2CH(CO_2^-)CH_2CH_2S(OOH)=CH_2$ or $NH_2CH(CO_2^-)CH_2CH=S(OOH)CH_3$ is formed by taking an H from the terminal $–SCH_3$ or from the γ-CH_2; neither of these two routes is facile.

Similar to gas-phase reactions, the first step of Met oxidation in solution is formation of persulfoxide. However, only in acidic solution the initially formed persulfoxide evolves to S-hydroperoxide; in basic solution, the structure of initial persulfoxide remains stable, presumably because of bulk solvent stabilization. In aqueous solution, persulfoxide or S-hydroperoxide could be thermalized through solute–solvent interactions. However, a downstream route opens for persulfoxide/S-hydroperoxide through the participation of other Met molecules, leading to sulfoxide.

Different from the gas-phase reactions where the reaction efficiencies mostly depend on the formation efficiencies of S-hydroperoxides, the reaction efficiencies in solution are also related to the second step, which leads to formation of sulfoxides by O-transfer between initially formed persulfoxide and second Met. Based on DFT-PCM calculations, the barriers for this reaction are 27.0, 25.1, and 38.6 kJ/mol for protonated, neutral, and deprotonated systems, respectively.

Conclusions

A new on-line reaction setup was developed to couple solution-phase reactions of electronically excited $^1O_2$ with an ESI mass spectrometer and an absorption spectrometer. This apparatus enables us to measure $^1O_2$ oxidation kinetics in aqueous solution. To determine $[^1O_2]$ in solution on an absolute scale, a method was established to correlate the $[^1O_2]$ in aqueous solution with airborne $^1O_2$ emission intensity. This on-line monitoring system was utilized to study the reaction kinetics of Met with $^1O_2$ at different pH. In both acidic and basic solutions, sulfoxide $[MetO - H]^-$ and $[MetO + H]^+$ were confirmed to be major products. We have captured the persulfoxide intermediates in basic solution. The reaction mechanism and pH dependence were elucidated with the assistance from DFT calculations, using the polarized continuum model to simulate bulk solvation effects. It was found that the reactions in acidic and basic media follow the same mechanism composed of two elementary steps, formation of persulfoxide for deprotonated Met or S-hydroperoxide for neutral/protonated Met, followed by transfer of an O atom from persulfoxide or S-hydroperoxide to a second Met, producing two sulfoxides. The second step is rate-limiting, and formation of sulfoxide follows third-order rate law with respect to $[Met]^2[^1O_2]$. A remarkable result concerns the pH dependence of Met oxidation. The effective rate constants for formation of Met sulfoxide are $3.7 \times 10^{10}\ M^{-2}\cdot s^{-1}$ at pH 3.2, decreasing to $1.0 \times 10^9\ M^{-2}\cdot s^{-1}$ at pH 10.4. The significantly lower rate constant in basic solution is due to the high activation barrier leading to formation of sulfoxide from deprotonated persulfoxide, and the latter overwhelmingly decayed back to reactants accompanied by physical quenching of $^1O_2$.

Combined with our findings in the gas-phase $^1O_2$ oxidation of hydrated/dehydrated Met ions, a panorama can be created for evolution of the Met oxidation mechanism from the gas phase, through microsolvation, to aqueous solution. Reactions in different media and at different ionization states are all mediated by persulfoxides, which carry high internal energy and thus are very reactive. In the gas phase, the fates of persulfoxides are determined by whether they have exit product channels or not. In the reaction of protonated Met, transfer of two H from $[Met + H]^+$ to O_2 provides an energetically favored dissociation path. To the contrary, H_2O_2 elimination is inhibited in deprotonated persulfoxide, and the latter could only decay back to reactants. The fates of persulfoxide intermediates are altered upon microsolvation in the gas phase. Dominant hydration effect is the suppression of persulfoxide decomposition. This can be attributed to energy dissipation from excited persulfoxide intermediates via water dissociation, yielding persulfoxides themselves as stable products. Finally, in solution-phase reactions, persulfoxide intermediates, once formed, continue to react with another molecule of Met, leading to formation of sulfoxides as final products.

Acknowledgments

The authors acknowledge support for this work by the National Science Foundation CAREER Award (Grant No. CHE-0954507), Queens College Research Enhancement Funds, and PSC-CUNY Research Awards.

References

1. Davies, M.J.: Singlet oxygen-mediated damage to proteins and its consequences. Biochem. Biophys. Res. Commun. **305**, 761–770 (2003)

2. Davies, M.J.: Reactive species formed on proteins exposed to singlet oxygen. Photochem. Photobiol. Sci. **3**, 17–25 (2004)
3. Davies, M.J.: The oxidative environment and protein damage. Biochim. Biophys. Acta **1703**, 93–109 (2005)
4. Lavine, T.F.: Formation, resolution, and optical properties of the diastereoisomeric sulfoxides derived from L-methionine. J. Biol. Chem. **169**, 477–491 (1947)
5. Vogt, W.: Oxidation of methionyl residues in proteins: tools, targets, and reversal. Free Radic. Biol. Med. **18**, 93–105 (1995)
6. Nielsen, H.K., Löliger, J., Hurrell, R.F.: Reactions of proteins with oxidizing lipids. 1. Analytical measurements of lipid oxidation and of amino acid losses in a whey protein-methyl linolenate model system. Br. J. Nutr. **53**, 61–73 (1985)
7. Valley, C.C., Cembran, A., Perlmutter, J.D., Lewis, A.K., Labello, N.P., Gao, J., Sachs, J.N.: The methionine-aromatic motif plays a unique role in stabilizing protein structure. J. Biol. Chem. **287**, 34979–34991 (2012)
8. Brot, N., Weissbach, L., Werth, J., Weissbach, H.: Enzymic reduction of protein-bound methionine sulfoxide. Proc. Natl. Acad. Sci. U. S. A. **78**, 2155–2158 (1981)
9. Caldwell, P., Luk, D.C., Weissbach, H., Brot, N.: Oxidation of the methionine residues of *Escherichia coli* ribosomal protein L12 decreases the protein's biological activity. Proc. Natl. Acad. Sci. U. S. A. **75**, 5349–5352 (1978)
10. Sacksteder, C.A., Whittier, J.E., Xiong, Y., Li, J., Galeva, N.A., Jacoby, M.E., Purvine, S.O., Williams, T.D., Rechsteiner, M.C., Bigelow, D.J., Squier, T.C.: Tertiary structural rearrangements upon oxidation of methionine145 in calmodulin promotes targeted proteasomal degradation. Biophys. J. **91**, 1480–1493 (2006)
11. Chao, C.-C., Ma, Y.-S., Stadtman, E.R.: Modification of protein surface hydrophobicity and methionine oxidation by oxidative systems. Proc. Natl. Acad. Sci. U. S. A. **94**, 2969–2974 (1997)
12. Garner, B., Waldeck, A.R., Witting, P.K., Rye, K.-A., Stocker, R.: Oxidation of high density lipoproteins II. Evidence for direct reduction of lipid hydroperoxides by methionine residues of apolipoproteins AI and AII. J. Biol. Chem. **273**, 6088–6095 (1998)
13. Levine, R.L., Mosoni, L., Berlett, B.S., Stadtman, E.R.: Methionine residues as endogenous antioxidants in proteins. Proc. Natl. Acad. Sci. U. S. A. **93**, 15036–15040 (1996)
14. Glaser, C., Schoeneich, C.: Special Issue: Methionine oxidation and methionine sulfoxide reductases. Elsevier B.V, Amsterdam, The Netherlands (2005) **[In: Biochim. Biophys. Acta; 2005, 1703(2)]**
15. Brot, N., Weissbach, H.: Biochemistry and physiological role of methionine sulfoxide residues in proteins. Arch. Biochem. Biophys. **223**, 271–281 (1983)
16. Grimaud, R., Ezraty, B., Mitchell, J.K., Lafitte, D., Briand, C., Derrick, P.J., Barras, F.: Repair of oxidized proteins: identification of a new methionine sulfoxide reductase. J. Biol. Chem. **276**, 48915–48920 (2001)
17. Drazic, A., Miura, H., Peschek, J., Le, Y., Bach, N.C., Kriehuber, T., Winter, J.: Methionine oxidation activates a transcription factor in response to oxidative stress. Proc. Natl. Acad. Sci. U. S. A. **110**, 9493–9498 (2013)
18. Erickson, J.R., Joiner, M.-lA., Guan, X., Kutschke, W., Yang, J., Oddis, C.V., Bartlett, R.K., Lowe, J.S., O'Donnell, S.E., Aykin-Burns, N., Zimmerman, M.C., Zimmerman, K., Ham, A.-J.L., Weiss, R.M., Spitz, D.R., Shea, M.A., Colbran, R.J., Mohler, P.J., Anderson, M.E.: A dynamic pathway for calcium-independent activation of CaMKII by methionine oxidation. Cell **133**, 462–474 (2008)
19. Pattison, D.I., Davies, M.J.: Absolute rate constants for the reaction of hypochlorous acid with protein side chains and peptide bonds. Chem. Res. Toxicol. **14**, 1453–1464 (2001)
20. Peskin, A.V., Winterbourn, C.C.: Kinetics of the reactions of hypochlorous acid and amino acid chloramines with thiols, methionine, and ascorbate. Free Radic. Biol. Med. **30**, 572–579 (2001)
21. Buxton, G.V., Greenstock, C.L., Helman, W.P., Ross, A.B.: Critical review of rate constants for reactions of hydrated electrons, hydrogen atoms, and hydroxyl radicals (·OH/·O^-) in aqueous solution. J. Phys. Chem. Ref. Data **17**, 513–886 (1988)
22. Matheson, I.B.C., He, J.: Chemical reaction rates of amino acids with singlet oxygen. photochem. Photobiology **29**, 879–881 (1979)
23. Miskoski, S., Garcia, N.A.: Influence of the peptide bond on the singlet molecular oxygen-mediated ($O_2[^1\Delta]$) photooxidation of histidine and methionine dipeptides. A kinetic study. Photochem. Photobiol. **57**, 447–452 (1993)
24. Sysak, P.K., Foote, C.S., Ching, T.-Y.: Chemistry of Singlet Oxygen. XXV. Photooxygenation of methionine. Photochem. Photobiol. **26**, 19–27 (1977)
25. Schweitzer, C., Schmidt, R.: Physical mechanisms of generation and deactivation of singlet oxygen. Chem. Rev. **103**, 1685–1757 (2003)
26. Weil, L., Gordon, W.G., Buchert, A.R.: Photooxidation of amino acids in the presence of methylene blue. Arch. Biochem. **33**, 90–109 (1951)
27. Spikes, J.D., MacKnight, M.L.: Dye-sensitized photooxidation of proteins. Ann. N. Y. Acad. Sci. **171**, 149–162 (1970)
28. Cohen, S.G., Ojanpera, S.: Photooxidation of methionine and related compounds. J. Am. Chem. Soc. **97**, 5633–5634 (1975)
29. Rougee, M., Bensasson, R.V., Land, E.J., Pariente, R.: Deactivation of singlet molecular oxygen by thiols and related compounds, possible protectors against skin photosensitivity. Photochem. Photobiol. **47**, 485–489 (1988)
30. Bertolotti, S.G., Garcia, N.A., Arguello, G.A.: Effects of the peptide bond on the singlet-molecular-oxygen-mediated sensitized photo-oxidation of tyrosine and tryptophan dipeptides. A kinetic study. J. Photochem. Photobiol. B **10**, 57–70 (1991)
31. Stadtman, E.R., Berlett, B.S.: Free-Radical-Mediated Modification of Proteins. In: Wallace, K.B. (ed.) Free Radical Toxicology, pp. 71–87. Taylor & Francis, Washington, DC (1997)
32. Frimer, A.A.: Singlet O_2. Vol III. Reaction Modes and Products, Part 2. CRC Press, Boca Raton, FL (1985)
33. Choudhury, R., Greer, A.: Synergism between airborne singlet oxygen and a trisubstituted olefin sulfonate for the inactivation of bacteria. Langmuir **30**, 3599–3605 (2014)
34. Bartusik, D., Aebisher, D., Ghafari, B., Lyons, A.M., Greer, A.: Generating singlet oxygen bubbles: a new mechanism for gas-liquid oxidations in water. Langmuir **28**, 3053–3060 (2012)
35. Fang, Y., Liu, F., Bennett, A., Ara, S., Liu, J.: Experimental and trajectory study on reaction of protonated methionine with electronically excited singlet molecular oxygen ($a^1\Delta_g$): reaction dynamics and collision energy effects. J. Phys. Chem. B **115**, 2671–2682 (2011)
36. Liu, F., Liu, J.: Oxidation dynamics of methionine with singlet oxygen: effects of methionine ionization and microsolvation. J. Phys. Chem. B **119**, 8001–8012 (2015)
37. Bonchio, M., Licini, G., Modena, G., Bortolini, O., Moro, S., Nugent, W.A.: Enantioselective Ti(IV) sulfoxidation catalysts bearing C3-symmetric trialkanolamine ligands: solution speciation by ^{1}H NMR and ESI-MS analysis. J. Am. Chem. Soc. **121**, 6258–6268 (1999)
38. Kang, Y.-B., Gade, L.H.: The nature of the catalytically active species in olefin dioxygenation with Phi(Oac)2: metal or proton? J. Am. Chem. Soc. **133**, 3658–3667 (2011)
39. Santos, L.S. (ed.): Reactive Intermediates: MS Investigations in Solution. Wiley-VCH Verlag GmbH & Co. KGaA, Weinheim (2010)
40. Yamashita, M., Fenn, J.B.: Negative ion production with the electrospray ion source. J. Phys. Chem. **88**, 4671–4675 (1984)
41. Wampler, F.M., Blades, A.T., Kebarle, P.: Negative ion electrospray mass spectrometry of nucleotides: ionization from water solution with SF_6 discharge suppression. J. Am. Soc. Mass Spectrom. **4**, 289–295 (1993)
42. Midey, A., Dotan, I., Viggiano, A.A.: Temperature dependences for the reactions of O^- and O_2^- with $O_2(a^1\Delta_g)$ from 200 to 700 K. J. Phys. Chem. A **112**, 3040–3045 (2008)
43. Liu, F., Fang, Y., Chen, Y., Liu, J.: Dissociative excitation energy transfer in the reactions of protonated cysteine and tryptophan with electronically excited singlet molecular oxygen ($a^1\Delta_g$). J. Phys. Chem. B **115**, 9898–9909 (2011)
44. Lafferty, W.J., Solodov, A.M., Lugez, C.L., Fraser, G.T.: Rotational line strengths and self-pressure-broadening coefficients for the 1.27 μm, $a^1\Delta_g$-$X^3\Sigma_g^-$, V = 0-0 Band of O_2. Appl. Opt. **37**, 2264–2270 (1998)
45. Lee, E.D., Muck, W., Henion, J.D., Covey, T.R.: Real-time reaction monitoring by continuous-introduction ion-spray tandem mass spectrometry. J. Am. Chem. Soc. **111**, 4600–4604 (1989)
46. Fürmeier, S., Metzger, J.O.: Detection of transient radical cations in electron transfer-initiated Diels-Alder reactions by electrospray ionization mass spectrometry. J. Am. Chem. Soc. **126**, 14485–14492 (2004)
47. Fabris, D.: Mass spectrometric approaches for the investigation of dynamic processes in condensed phase. Mass Spectrom. Rev. **24**, 30–54 (2005)
48. Amarante, G.W., Benassi, M., Milagre, H.M.S., Braga, A.A.C., Maseras, F., Eberlin, M.N., Coelho, F.: Brønsted acid catalyzed Morita–Baylis–Hillman reaction: a new mechanistic view for thioureas revealed by ESI-MS(/MS) monitoring and DFT calculations. Chem. Eur. J. **15**, 12460–12469 (2009)

49. Huvaere, K., Sinnaeve, B., Bocxlaer, J.V., Skibsted, L.H.: Flavonoid deactivation of excited state flavins: reaction monitoring by mass spectrometry. J. Agric. Food Chem. **60**, 9261–9272 (2012)
50. Yunker, L.P.E., Stoddard, R.L., McIndoe, J.S.: Practical approaches to the ESI-MS analysis of catalytic reactions. J. Mass Spectrom. **49**, 1–8 (2014)
51. Yan, X., Sokol, E., Li, X., Li, G., Xu, S., Cooks, R.G.: On-line reaction monitoring and mechanistic studies by mass spectrometry: Negishi cross-coupling, hydrogenolysis, and reductive amination. Angew. Chem. Int. Ed. **53**, 5931–5935 (2014)
52. Liu, F., Lu, W., Fang, Y., Liu, J.: Evolution of oxidation dynamics of histidine: non-reactivity in the gas phase, peroxides in hydrated clusters, and pH dependecne in solution. Phys. Chem. Chem. Phys. **16**, 22179–22191 (2014)
53. Cassou, C.A., Sterling, H.J., Susa, A.C., Williams, E.R.: Electrothermal supercharging in mass spectrometry and tandem mass spectrometry of native proteins. Anal. Chem. **85**, 138–146 (2013)
54. Mark, L.P., Gill, M.C., Mahut, M., Derrick, P.J.: Dual nano-electrospray for probing solution interactions and fast reactions of complex biomolecules. Eur. J. Mass Spectrom. **18**, 439–466 (2012)
55. Fisher, C.M., Kharlamova, A., McLuckey, S.A.: Affecting protein charge state distributions in nano-electrospray ionization via in-spray solution mixing using Theta capillaries. Anal. Chem. **86**, 4581–4588 (2014)
56. Mortensen, D.N., Williams, E.R.: Theta-glass capillaries in electrospray ionization: rapid mixing and short droplet lifetimes. Anal. Chem. **86**, 9315–9321 (2014)
57. Fang, Y., Liu, J.: Reaction of protonated tyrosine with electronically excited singlet molecular oxygen ($a^1\Delta_g$): an experimental and trajectory study. J. Phys. Chem. A **113**, 11250–11261 (2009)
58. Armentrout, P.B.: Fundamental of ion-molecule chemistry. J. Anal. At. Spectrom. **19**, 571–580 (2004)
59. Frisch, M.J., Trucks, G.W., Schlegel, H.B., Scuseria, G.E., Robb, M.A., Cheeseman, J.R., Scalmani, G., Barone, V., Mennucci, B., Petersson, G.A., Nakatsuji, H., Caricato, M., Li, X., Hratchian, H.P., Izmaylov, A.F., Bloino, J., Zheng, G., Sonnenberg, J.L., Hada, M., Ehara, M., Toyota, K., Fukuda, R., Hasegawa, J., Ishida, M., Nakajima, T., Honda, Y., Kitao, O., Nakai, H., Vreven, T., Montgomery, J.A., Peralta, J.E., Ogliaro, F., Bearpark, M., Heyd, J.J., Brothers, E., Kudin, K.N., Staroverov, V.N., Keith, T., Kobayashi, R., Normand, J., Raghavachari, K., Rendell, A., Burant, J.C., Iyengar, S.S., Tomasi, J., Cossi, M., Rega, N., Millam, J.M., Klene, M., Knox, J.E., Cross, J.B., Bakken, V., Adamo, C., Jaramillo, J., Gomperts, R., Stratmann, R.E., Yazyev, O., Austin, A.J., Cammi, R., Pomelli, C., Ochterski, J.W., Martin, R.L., Morokuma, K., Zakrzewski, V.G., Voth, G.A., Salvador, P., Dannenberg, J.J., Dapprich, S., Daniels, A.D., Farkas, O., Foresman, J.B., Ortiz, J.V., Cioslowski, J., Fox, D.J.: Gaussian 09, Revision D.01. Gaussian, Inc, Wallingford, CT (2013)
60. Tomasi, J., Mennucci, B., Cammi, R.: Quantum mechanical continuum solvation models. Chem. Rev. **105**, 2999–3093 (2005)
61. Zou, X., Zhao, H., Yu, Y., Su, H.: Formation of guanine-6-sulfonate from 6-thioguanine and singlet oxygen: a combined theoretical and experimental study. J. Am. Chem. Soc. **135**, 4509–4515 (2013)
62. Munk, B.H., Burrows, C.J., Schlegel, H.B.: An exploration of mechanisms for the transformation of 8-oxoguanine to guanidinohydantoin and spiroiminodihydantoin by density functional theory. J. Am. Chem. Soc. **130**, 5245–5256 (2008)
63. Alecu, I.M., Zheng, J., Zhao, Y., Truhlar, D.G.: Computational thermochemistry: scale factor databases and scale factors for vibrational requencies obtained from electronic model chemistries. J. Chem. Theory Comput. **6**, 2872–2887 (2010)
64. Skovsen, E., Snyder, J.W., Lambert, J.D.C., Ogilby, P.R.: Lifetime and diffusion of singlet oxygen in a cell. J. Phys. Chem. B **109**, 8570–8573 (2005)
65. Lindig, B.A., Rodgers, M.A.J., Schaap, A.P.: Determination of the lifetime of singlet oxygen in D_2O using 9,10-anthracenedipropionic acid, a water-soluble probe. J. Am. Chem. Soc. **102**, 5590–5593 (1980)
66. Kanofsky, J.R.: Quenching of singlet oxygen by human plasma. Photochem. Photobiol. **51**, 299–303 (1990)
67. Fischer, F., Graschew, G., Sinn, H.J., Maier-Borstl, W., Lorenzl, W.J., Schlag, P.M.: A chemical dosimeter for the determination of the photodynamic activity of photosensitizers. Clin. Chim. Acta **274**, 89–104 (1998)
68. Montaña, M.P., Massad, W.A., Amat-Guerri, F., García, N.A.: Scavenging of riboflavin-photogenerated oxidative species by uric acid, xanthine or hypoxanthine: a kinetic study. J. Photochem. Photobiol. A **193**, 103–109 (2008)
69. Krasnovsky, A.A., Kozlov, A.S., Roumbal, Y.V.: Photochemical investigation of the IR absorption bands of molecular oxygen in organic and aqueous environment. Photochem. Photobiol. Sci. **11**, 988–997 (2012)
70. Rabello, B.R., Gerola, A.P., Pellosi, D.S., Tessaro, A.L., Aparício, J.L., Caetano, W., Hioka, N.: Singlet oxygen dosimetry using uric acid as a chemical probe: systematic evaluation. J. Photochem. Photobiol. A **238**, 53–62 (2012)
71. Voet, D., Voet, J.G., Pratt, C.W.: Fundamentals Biochemistry (Upgrade Edition). John Wiley & Sons, Inc., Hoboken, NJ (2002)
72. Block, E., O'Connor, J.: Chemistry of alkyl thiosulfinate esters. VI. Preparation and spectral studies. J. Am. Chem. Soc. **96**, 3921–3929 (1974)
73. Foote, C.S., Peters, J.W.: Chemistry of singlet oxygen. XIV. Reactive Intermediate in sulfide photooxidation. J. Am. Chem. Soc. **93**, 3795–3796 (1971)
74. Liang, J.J., Gu, C.L., Kacher, M.L., Foote, C.S.: Chemistry of singlet oxygen. 45. Mechanism of the photooxidation of sulfides. J. Am. Chem. Soc. **105**, 4717–4721 (1983)
75. Steinfeld, J.I., Francisco, J.S., Hase, W.L.: Chemcial Kinetcis and Dynamics, 2nd edn. Prentice Hall, Upper Saddle River, NJ (1999)
76. Clennan, E.L.: Persulfoxide: key intermediate in reactions of singlet oxygen with sulfides. Acc. Chem. Res. **34**, 875–884 (2001)
77. Silbey, R.J., Alberty, R.A., Bawendi, M.G. Physical Chemistry, 4th ed. Wiley, Hoboken, NJ (2005)
78. Kraljic, I., Sharpatyi, V.A.: Determination of singlet oxygen rate constants in aqueous solutions. Photochem. Photobiol. **28**, 583–586 (1978)
79. Lindig, B.A., Rodgers, M.A.J.: Rate parameters for the quenching of singlet oxygen by water-soluble and lipid-soluble substrates in aqueous and micellar systems. Photochem. Photobiol. **33**, 627–634 (1981)
80. Weil, L.: On the mechanism of the photo-oxidation of amino acids sensitized by methylene blue. Arch. Biochem. Biophys. **110**, 57–68 (1965)
81. Straight, R., Spikes, J.D.: Sensitized photooxidation of amino acids: effects on the reactivity of their primary amine groups with fluorescamine and O-phthalaldehyde. Photochem. Photobiol. **27**, 565–569 (1978)